Cellular Pressure and Volume Regulation and Implications for Cell Mechanics

Hongyuan Jiang[†] and Sean X. Sun[†‡*]
[†]Department of Mechanical Engineering and [‡]Department of Biomedical Engineering and Johns Hopkins Physical Oncology Center, Johns Hopkins University, Baltimore, Maryland

ABSTRACT In eukaryotic cells, small changes in cell volume can serve as important signals for cell proliferation, death, and migration. Volume and shape regulation also directly impacts the mechanics of cells and tissues. Here, we develop a mathematical model of cellular volume and pressure regulation, incorporating essential elements such as water permeation, mechanosensitive channels, active ion pumps, and active stresses in the cortex. The model can fully explain recent experimental data, and it predicts cellular volume and pressure for several models of cell cortical mechanics. Moreover, we show that when cells are subjected to an externally applied load, such as in an atomic force microscopy indentation experiment, active regulation of volume and pressure leads to a complex cellular response. Instead of the passive mechanics of the cortex, the observed cell stiffness depends on several factors working together. This provides a mathematical explanation of rate-dependent response of cells under force.

INTRODUCTION

Unlike plant and bacterial cells, animal cells lack a stiff cell wall that resists large changes in cell volume. Instead, the interplay of membrane tension, active contractility, water, and ion flows control the cell shape and volume (1). Conversely, when external forces are applied to the cell, the observed shape and pressure responses are also the combined results of these influences. A quantitative understanding of this important system is still lacking. Most mathematical models of cell-shape dynamics treat the cell as a constant volume of cytoplasm surrounded by a layer of membrane or cortex (see more detailed review in Clark and Paluch (2) and Sabreux et al. (3)). Such models have been successfully used to quantitatively describe problems such as red blood cell mechanics (4) and shape instability of dividing cells (5). However, the transport of water and ions and the subsequent cell-volume change controlled by passive or active ion channels are generally neglected in these models. In studies of cell mechanics with mechanical perturbation measurements (6–9), cells are usually modeled as an elastic or viscoelastic body, without consideration of the possible volume change induced by external forces. Lately, however, cell-volume dynamics is being recognized as an important element in cell mechanics. A recent experiment (10) showed that cell rheological properties can change due to the effects of the interstitial fluid and related volume change. Another recent experiment (11) measured volume and pressure changes in metaphase cells after introducing osmotic shocks. The quantitative results of that experiment showed that the cell volume during metaphase can adapt to large external osmotic shocks, and that the adaptation timescale is over tens of minutes. There are large numbers of studies on ion channels in cell osmotic regulation, and cell mechanics. However, there seem to be a limited number of studies so far linking these two fundamental aspects. Here we develop a mathematical model of cell volume and pressure response, combining the influence of cortical tension, water permeation, and ion dynamics. The model is able to compute cell-shape changes during osmotic shock and predict the response of the cell to externally applied mechanical forces. We show that the mechanical response of cells during slow deformations (~μm/min) is dominated by water permeation. Cytoskeletal mechanics is only one of several variables that strongly influence the apparent cellular mechanical response.

Cytoplasmic fluid flow has been examined as an important element that controls the overall mechanics of eukaryotic animal cells (12), and a recent experiment showed that the cytoplasm of living cells behaves as a poroelastic material (10) where fluid pressure gradients equilibrate on the scale of tens of seconds. A closely related phenomenon is cellular blebs, where local build up of hydrostatic pressure leads to detachment of the membrane from the actomyosin cortex underneath the membrane (13). The developed bleb bulges out from the cell, and in some cases, the cortex can reform. Blebbing has been observed during cytokinesis (5) and has been implicated in amoeba cell motility (13). Less attention has been paid to how cytoplasmic fluid might flow across the cell membrane. Indeed, the cell membrane is permeable to a variety of ions, small solutes, and water.

Submitted April 15, 2013, and accepted for publication June 12, 2013.

*Correspondence: ssun@jhu.edu

Hongyuan Jiang's present address is Department of Modern Mechanics, University of Science and Technology of China, Hefei, Anhui 230026, PRC

Editor: Charles Wolgemuth.

0006-3495/13/08/0609/11 $2.00

http://dx.doi.org/10.1016/j.bpj.2013.06.021

Therefore, both hydrostatic and osmotic pressures control fluid flow across the membrane. Since water is essentially incompressible, the flow of fluid is directly related to cell volume change. This phenomenon is typically seen when cells are subjected to large osmotic shocks. Equally important, ion and osmolyte flow across membrane channels and pumps can also change osmotic pressure. Flows of small molecules and ions across the membrane are principally controlled by two types of membrane proteins. Mechanosensitive channels are passive membrane proteins that can open in response to changes in membrane tension. Subsequent ion flows across the channel are driven by concentration differences. In contrast, active ion pumps are energy-consuming membrane proteins that pump solutes and ions against concentration gradients. Finally, the actomyosin cortex underneath the membrane and the active stress generated by molecular motors can also influence membrane tension and cellular hydrostatic pressure, indirectly influence solute and ion flow, and thus influence the cell volume. The membrane tension will also influence the opening and closing of mechanosensitive channels. One experiment (11) revealed that when the cortex is disrupted with blebbistatin to inhibit myosin II contraction and latrunculin A to depolymerize actin filaments, the volume of mitotic cells slightly increases. Therefore, all of these elements must be considered together to understand cell shape and pressure changes.

Understanding the combined effects of water, ions, cytoskeletal mechanics, and contractility is important for understanding the overall mechanical response of cells, tissues, and developmental mechanics in general. There are now experiments utilizing atomic force microscopy (AFM) or microrheology to measure the mechanical response of the cell (6–9). When forces are applied to the cell, hydrostatic pressure and cortical tension can change, leading to changes in water and ion flow. We use our model to compute the shape and force response of the cell during a constant-velocity indentation. The results reveal the underlying molecular mechanism that controls the rate-dependent viscoelastic response of the cell. More generally, it has been proposed that by placing the membrane channels and pumps nonuniformly, the cell can introduce influx and efflux of water at different locations (14,15). This mechanism may be crucial for cell motility in neutrophils, and may be important in cell-shape changes in general.

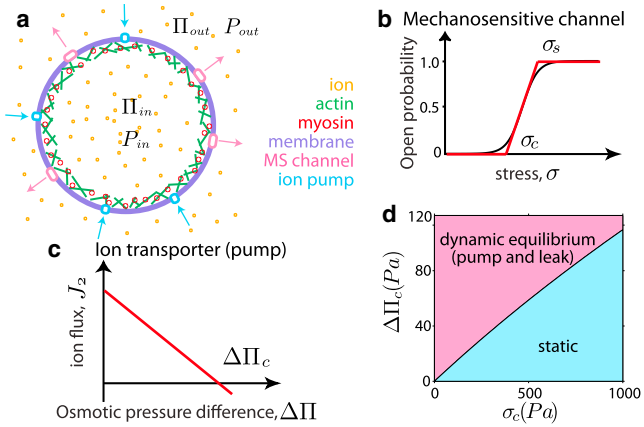

FIGURE 1 (*a*) A minimal model of cell volume and pressure regulation. We consider a spherical cell enclosed by an actomyosin cortex and the cell membrane. Embedded in the membrane are several families of passive MS ion channels and active ion pumps. The MS channels and active ion pumps can change the internal ion concentration, c_{in}, and the intneral osmotic pressure, Π_{in}, leading to changes in water flux across the membrane. Net flow of water leads to cell volume changes. (*b*) Opening probability versus cortical stress for an MS channel. The red curve shows the simplified piecewise linear function used in Eq. 2. (*c*) The flux of ions transported by ion transporters as a function of osmotic pressure difference, $\Delta\Pi$. This flux is modeled by Eq. 3. (*d*) The steady-state phase diagram of the cell as a function of model parameters $\Delta\Pi_c$ and σ_c. The model predicts two regimes. In the static regime, there are no ion fluxes at steady-state cell size. All of the channels and pumps are inactive. In the pump-and-leak regime, the influx and efflux of ions balance, and the cell maintains a steady-state size.

A MINIMAL MODEL OF CELLULAR VOLUME AND PRESSURE REGULATION

Let us consider a minimal model of volume and pressure regulation for a spherical cell, e.g., a mitotic cell or a cell in suspension. The cellular cytoplasm is enclosed by a cortical layer, which is a network of actin filaments and contractile myosin motors (Fig. 1 *a*). Enclosing and adhering to the cortex is one layer of cell membrane, in which passive mechanosensitive (MS) ion channels and active ion transporters are embedded. The mechanical tension in the membrane is a complex issue. The overall membrane tension is controlled by the hydrostatic pressure difference across the membrane, membrane-cytoskeleton adhesion, and active stresses in the cell cortex. However, the tension is also known to be related to the total membrane area, and therefore is also regulated by membrane superstructures (e.g., membrane folds and blebs) and membrane trafficking (e.g., exocytosis and endocytosis) (16). In particular, when the hydrostatic pressure in the cell becomes large, the membrane may detach from the cortex, leading to the formation of cellular blebs (17). Therefore, the cortical tension is not necessarily equivalent to the membrane tension. Here, to simplify the problem, we neglect the membrane superstructures and membrane trafficking, and treat the cell membrane and cortex as a single mechanical structure.

Kinetics of water

Let P_{in} and Π_{in} be the hydrostatic pressure and the osmotic pressure, respectively, inside the spherical cell. The corresponding values in the extracellular environment are P_{out} and Π_{out} (Fig. 1 *a*). Osmotic pressure can be estimated using the Van't Hoff equation $\Pi = cRT$, where c is the molar concentration of solutes, R is the gas constant, and T is absolute temperature. For an enclosed volume, this can be written as $\Pi V = nRT$, where V is the net volume and n is the total

number of solutes. For high solute concentrations and crowded cellular environments, the osmotic pressure is similar, except that one should include an activity coefficient that measures the deviation away from the ideal solution approximation above. The chemical potential of water on both sides is given by $\Psi_{in} = P_{in} - \Pi_{in}$ and $\Psi_{out} = P_{out} - \Pi_{out}$. Therefore, the flux of water can be modeled as $J_{water} = -\alpha\Delta\Psi$ (18), where α is a rate constant, $\Delta\Psi = (\Delta P - \Delta\Pi)$ is the chemical potential difference, and $\Delta P = P_{in} - P_{out}$ and $\Delta\Pi = \Pi_{in} - \Pi_{out}$ are the hydrostatic and osmotic pressure differences across the membrane. The volume change of a spherical cell with radius r is then $d/dt((4/3)\pi r^3) = 4\pi r^2 J_{water}$, which gives

$$\frac{dr}{dt} = J_{water} = -\alpha(\Delta P - \Delta\Pi). \quad (1)$$

In some cells, membrane water permeability can be enhanced by aquaporins, also known as water channels (19). This additional mechanism for water transport simply increases the constant α in our model. Thus, the permeability constant α is related to both the basal permeability of the cell membrane and water flux through specialized water channels.

Kinetics of ions and small molecules

In a vesicle enclosed by a semipermeable membrane, the flux of solutes is zero and the flux of water is sufficient to describe the volume change. In living cells, there are many mechanosensitive (MS) channels (20) and active ion and small-molecule transporters (or pumps) (21,22) in the cell membrane, which enable the cell to actively control the influx and efflux of ions and other osmolytes. Therefore, the kinetics of the solute must be included to study the volume and pressure regulation of living cells. To reduce complexity, we include only one species of MS channel and one species of ion transporter in our model.

MS channels are membrane proteins that can open a pore in response to mechanical stimuli (20). They act as emergency valves to release solutes in response to hypotonic shocks. These channels can vary in permittivity from nonselective to highly selective (20). The opening probability, P_{open}, of MS channels follows a Boltzmann function (23) (Fig. 1 *b*). If there are N MS channels on the cell membrane, and there are NP_{open} open channels for a given stress. Therefore, the ion flux across MS channels is proportional to $NP_{open}\Delta c/h_0$, where $\Delta c/h_0$ represents the concentration gradient of ions, and h_0 is the membrane thickness. By approximating the Boltzmann function by a piecewise linear function (Fig. 1 *b*, *red curve*), the ion flux due to the opening of MS channels can be modeled as

$$J_1 = \begin{cases} 0 & \text{if } \sigma \le \sigma_c \\ -\beta(\sigma - \sigma_c)\Delta\Pi & \text{if } \sigma_c < \sigma < \sigma_s \\ -\beta(\sigma_s - \sigma_c)\Delta\Pi & \text{if } \sigma \ge \sigma_s \end{cases}, \quad (2)$$

where β is a rate constant. σ_c is the threshold stress, below which J_1 is zero. σ_s is the saturating stress, above which all MS channels are open. Here, Δc is replaced by $\Delta\Pi$ since $\Delta\Pi = RT\Delta c$. The coefficients RT and h_0 can be absorbed by β.

MS channels release ions passively in the direction of the concentration gradient, whereas ion transporters (or ion pumps), the other type of transmembrane protein, are used by cells to actively import ions across a plasma membrane against a concentration or electrochemical gradient (21,22). Ion transporters require the input of energy, such as from ATP hydrolysis, energy-releasing enzymatic reactions, or sunlight, to overcome the energy barrier from an ion concentration or electrochemical gradient. For simplicity, here we consider only a concentration gradient. The free-energy change during the pumping action is $\Delta G = RT\log(c_{in}/c_{out}) - \Delta G_a$, where c_{in} and c_{out} are the ion concentrations inside and outside the cell, respectively. In most cases, $c_{in} > c_{out}$ and the first term of ΔG is positive. Therefore, the process is unfavorable and must require energy input ΔG_a, which typically can come from energy sources such as ATP. It should be noted that since we only have one species of ion in this model, we neglect the charge of ions and the requirement of electroneutrality. In general, however, it is also possible to generalize to multiple ionic species and examine possible changes in the cell voltage with volume by adding an electrical potential term in the free-energy change described above (24). The ion flux across transporters can be modeled as $J_2 = -\gamma'\Delta G$, where γ' is a permeation constant. By assuming $c_{in} - c_{out} \ll c_{in}$, we can perform a Taylor expansion and ΔG can be linearized as $\Delta G = RT(c_{in} - c_{out})/c_{out} - \Delta G_a = RT(\Pi_{in} - \Pi_{out})/\Pi_{out} - \Delta G_a$. Thus, the flux by active pumping of ion transporters can be written as (Fig. 1 *c*)

$$J_2 = \gamma(\Delta\Pi_c - \Delta\Pi), \quad (3)$$

where γ is a constant. $\Delta\Pi_c = \Pi_{out}\Delta G_a/RT$ is a critical osmotic pressure difference, which is given by $\Delta G = 0$. The free energy from ATP during typical cellular conditions is ~30 kJ/mol, and the osmotic pressure of the medium is $\Pi_{out} = 0.5$ MPa (17), which yields $\Delta\Pi_c \approx 6 \times 10^4 \Pi_{out} \approx 3 \times 10^4$MPa. It should be noted that the active transport is a complex process that involves multistep enzymatic reactions (25). The expression and activity of ion transporters are influenced by other regulators and ATP/ADP concentrations (25). There are also multiple species of transporters, and the actual values of $\Delta\Pi_c$ would vary depending on the energy source and the molecular mechanism.

Notice that in our article, efflux is negative and influx is positive (Eqs. 2 and 3). Given J_1 and J_2, the total number of ions in a spherical cell is determined by

$$\frac{dn}{dt} = 4\pi r^2(J_1 + J_2). \quad (4)$$

Force balance and the mechanics of the cell cortex

We consider the situation where the hydrostatic pressure inside the cell is sufficiently low that the cell membrane is attached to the cell cortex, and there is no blebbing (17). Furthermore, we neglect the dynamics of membrane superstructures and membrane trafficking (16). Therefore, the cortex and membrane can be treated as a single layer. For a spherical cell, from mechanical force balance, the overall cortical stress is given by $\sigma = \Delta P r/2h$, where h is the cortical thickness. The mechanics of the cell cortex is interesting and complex. Models such as the active gel model (26,27) have been developed to describe the cortical mechanics. Elastic cortex models have also been used under certain situations (2,5,17,28). In general, the constitutive law of the cortex can be written as $\sigma = \sigma_p - \sigma_a$, where σ_a is the active stress from the contraction of myosin motors, and σ_p is the passive stress from deformation of the actin network (26,27). Note that because myosin applies a contractile force on the actin filament network, σ_a is negative.

In this article, based on elastic cortex models (2,5,17,28), we first focus on a more general viscoelastic model. In this case, the passive stress can be written as $\sigma_p = K/2\,(S/S_0 - 1) + \eta(1/S)(dS/dt)$, where K is the elastic modulus and η is the viscosity of the cortex. S and S_0 are the deformed and reference surface areas, respectively. The constitutive law is then

$$\sigma = \frac{K}{2}\left(\frac{S}{S_0} - 1\right) + \eta\frac{1}{S}\frac{dS}{dt} - \sigma_a \quad (5)$$

For a spherical cell, this is reduced to $\sigma = K/2\,(r^2/r_0^2 - 1) + \eta(2/r)(dr/dt) - \sigma_a$, where r and r_0 are the cell radii in the deformed and reference states, respectively. In a typical experiment (11), the cell radius changes $\sim 10\%$ in several minutes, and the apparent viscosity of the cortex is given by $\eta \approx 10^2 \sim 10^3$Pa·s (4,29). Thus, $\eta(2/r)(dr/dt) \approx 10^{-1} \sim 10^0$Pa, which is much smaller than the other terms in Eq. 5. Therefore, in this problem, the contribution of the viscous term $\eta(2/r)(dr/dt)$ is negligible. In this case, our viscoelastic model is reducible to an elastic cortex model (2,17,28).

RESULTS

Cells pump and leak

Using Eq. 5 and solving the coupled equations above (Eqs. 1–4), we find that the model yields a steady cell radius. However, there exist two different regimes (Fig. 1 *d*). In one regime, $\Delta\Pi_c$ is so small that the energy provided by ΔG_a can only overcome a small concentration gradient. However, the ion concentration difference does not generate enough hydrostatic pressure to activate MS channels. Therefore, at steady state, the flux through both MS channels and ion transporters is zero (Fig. S2) and the cell is static. In contrast, if $\Delta\Pi_c$ is sufficiently large, MS channels will be activated before the influx through ion transporters decreases to zero. So there should be a dynamic equilibrium (Fig. S1) where influx and efflux balance and the net ion flux is zero. This regime is consistent with the so-called pump-leak concept: there is an active influx of ions balanced by a passive leak of these ions in the opposite direction (1,25). For the constitutive law in Eq. 5, cells pump and leak when

$$\Delta\Pi_c > \frac{2h\sigma_c\sqrt{K}}{r_0\sqrt{K + 2(\sigma_c + \sigma_a)}}. \quad (6)$$

For the parameter range of the living cells summarized in Table 1, we find that the above condition becomes $\Delta\Pi_c >$ 90 Pa. For ATP-driven pumps, $\Delta\Pi_c \approx 3 \times 10^4$MPa, as discussed above. This implies that Eq. 6 is always satisfied for a typical cell in metaphase. Therefore, cells in Stewart et al. (11) are in the pump-and-leak regime. It should be noted that the static regime is an idealization. If we use the Boltzmann distribution proposed in Sukharev et al. (23), there should be three regimes: the saturated efflux regime, the quasistatic regime, and the intermediate regime. In the quasistatic regime, the efflux of ions is much smaller than that in the other regimes but is not zero. In this case, the boundary between the two regimes is no longer the sharp interface depicted in Fig. 1 *d*.

Cells can adapt to osmotic shocks

After applying a hypotonic shock to a cell that is initially in dynamic equilibrium (Fig. 2 *a*), the decrease of medium osmotic pressure drives the influx of water. The influx of water leads to an increase of both the cell radius (volume) and hydrostatic pressure difference. The influx of water also leads to an increase of cortical stress, which in turn opens more MS channels and increases the efflux of ions. Therefore, the net ion flux becomes negative (efflux), so that the total number of ions, n, decreases. As n decreases, the cortical stress and the efflux of ions decrease. When $\Delta\Pi < \Delta P$, water flows out of the cell again. The hydrostatic pressure difference and cell radius (volume) decrease and finally return to their original value (Fig. 2, *d* and *e*). The net change is a decrease in the total number of ions, n (Fig. 2 *g*), and the osmotic pressure inside the cell, Π_{in} (Fig. 2 *b*). Conversely, when hypertonic shock is introduced (Fig. 2 *a*), water flows out, so that the cell volume and the hydrostatic pressure decrease, and the cortical stress decreases. An increasing number of MS channels are closed. If the

TABLE 1 Summary of parameters used in the calculations

Parameter	Description	Value from experiments	Value in simulation
h	Thickness of cortical layer (μm)	$0.1 \sim 0.6$ (17,41)	0.5
K	Elastic constant of the cortical layer (KPa)	$10^{-1} \sim 10^{2}$ (42)	6
σ_a	Active stress inside the cortex (Pa)	-100	-100
σ_c	Threshold stress of MS channel (Pa)	-	300[a]
σ_s	Saturating stress of MS channel (Pa)	-	900[a]
$\Delta\Pi_c$	Critical osmotic pressure difference of ion pump (GPa)	-	30[b]
r_0	Cell radius in the reference state (μm)	8.5 (17)	8
Π_{out}	Osmotic pressure outside the cell (MPa)	0.5 (17)	0.5
α	Rate constant of water transport ($m \cdot s^{-1}\ Pa^{-1}$)	10^{-9}[c]	10^{-9}
γ	Rate constant of ion flux across ion transporters ($mol \cdot m^{-2}\ s^{-1}\ Pa^{-1}$)	$10^{-16} \sim 10^{-17}$ (43,44)[d]	10^{-17}
β	Rate constant of ion flux across MS channels ($mol \cdot m^{-2}\ s^{-1}\ Pa^{-2}$)	$10^{-11} \sim 10^{-10}$[e]	2×10^{-11}

[a]The mechanosensitive channel of large conductance (MscL) follows a Boltzmann distribution with midpoint tension (50% of the channel being open) at 12 dyn cm^{-1} (23). The threshold tension of MscL, which is defined as the pressure at which openings are readily observed every 0.5–2 s in experiments, is much lower. The MS channel of small conductance (MscS) has an even lower threshold tension. MscL and MscS are MS channels in prokaryotic cells. In eukaryotic cells, the threshold tension is much lower (20). Our model is mainly used to describe the volume regulation of eukaryotic cells. Therefore, we estimate a small threshold stress for MS channels here. The saturating stress of the MS channel is assumed to be three times its threshold stress.

[b]See our estimate in the main text.

[c]Across various eukaryotic cells, the permeability rate, P_f, is usually reported in the range $10^{-5} \sim 10^{-4}$ m/s (45). The definition of the water permeability rate relates the flux created by a concentration, $J = P_f V_w \Delta c = (P_f V_w/RT)\Delta\Pi$, where V_w is the molar volume of water, Δc is the difference of concentration across the membrane, and $\Delta\Pi$ is the osmotic pressure difference across the membrane. From this relation, we can get $\alpha = P_f V_w/RT$. Therefore, $\alpha = 10^{-13} \sim 10^{-12}\ m \cdot s^{-1}\ Pa^{-1}$. We found that if we use $\alpha = 10^{-12}\ m \cdot s^{-1}\ Pa^{-1}$, the adaptation time is ~100 min, which is longer than the experimentally observed adaptation time (several minutes). We found water channels can be used to reconcile this discrepancy. Water channels, also known as aquaporins, are found to significantly increase the water permeability in many cells (19). The water permeability of these types of cells is much larger than the permeability by simple diffusion through the plasma membrane. In fact, the experimentally measured water permeability (45,46) is the diffusional water permeability or basal permeability, i.e., the permeability in the absence of any specific transport pathway. In other words, the contribution of water channels has been excluded in these experiments. The existence of water channels will increase the rate of water transport and the constant α in our model. In the simulation, we found that the adaptation time is not very sensitive to α, since the adaptation time changes by one order of magnitude (from several minutes to ~100 minutes) as α changes by three orders of magnitude (from $10^{-9}\ m \cdot s^{-1}\ Pa^{-1}$ to $10^{-12}\ m \cdot s^{-1}\ Pa^{-1}$). We also found that the simulation is quite consistent with the experimental results when $\alpha = 10^{-9}\ m \cdot s^{-1}\ Pa^{-1}$. Therefore, α can be regarded as a fitting parameter in this work.

[d]The flux of the sodium ion on active transport of Na^+ is $\sim 10^{-7} \sim 10^{-6}\ mol \cdot m^{-2}\ s^{-1}$ (43,44). This number is quite close to our calculated ion flux across pumps, which has a maximum at $\sim 10^{-7}\ mol \cdot m^{-2}\ s^{-1}$. Divided by $\Delta\Pi_c$, the rate constant γ in our model is $\sim 10^{-16} \sim 10^{-17}\ mol \cdot m^{-2}\ s^{-1}$.

[e]The ion flux due to the opening of MS channels has an amplitude similar to that of the ion flux across ion pumps, i.e., $10^{-7} \sim 10^{-6}\ mol \cdot m^{-2}\ s^{-1}$ (43,44) for Na^+. Normalized by σ_c and $\Delta\Pi$, the rate constant β in our model is estimated as $10^{-11} \sim 10^{-10}\ mol \cdot m^{-2}\ s^{-1}\ Pa^{-1}$.

hypertonic shock is sufficiently large that $\sigma < \sigma_c$ (Fig. 2 *f*), then all the MS channels are closed ($J_{out} = 0$) (Fig. 2 *j*). Therefore, the net ion flux becomes positive (influx), so that the total number of ions, n, increases. As n increases, the cortical stress and efflux of ions increase. When $\Delta\Pi > \Delta P$, water enters the cell again. After that, the cell can gradually recover to the original hydrostatic pressure difference and cell radius (Fig. 2, *d* and *e*). Notice that the time courses of adaptation to hypotonic and hypertonic shock are different. This is because when all MS channels are closed, the speed of the recovery is limited. This could be one of the reasons that the time needed to recover from hypertonic shock is longer (11); more sophisticated experiments are required to test this prediction.

In Fig. 2, we assume that $\Delta\Pi_c$ is a constant, $\Delta\Pi_c = 6 \times 10^{10}$ Pa. Cells can exactly recover their original volume. In general, however, $\Delta\Pi_c$ should depend on Π_{out}, as discussed earlier. If we adopt this assumption and use $\Delta\Pi_c = 3 \times 10^4 \Pi_{out}$, imperfect adaptation to osmotic shocks occurs (Fig. 3). The steady-state values of r and ΔP become slightly smaller after the hypotonic shock, whereas they become slightly larger after the hypertonic shock.

Cells can actively adjust the adaptation level

In our model, the steady-state size of the cell is determined by a combination of parameters. Cells can potentially control these parameters to achieve different sizes. In the experiment (11), when ion pumps, e.g., Na^+/H^+ antiporters, are blocked by ethylisopropylamiloride (EIPA), both cell volume and pressure decrease. In our model, we use a decrease in $\Delta\Pi_c$, i.e., there is a lowering of ion pump performance, to describe the inhibition of Na^+/H^+ antiporters by EIPA (Fig. S3). In the experiment (11), rendering the membrane more permeable to ions by pore-forming α-toxin or HlyA also leads to a decrease of the cell volume and pressure. We can simulate this result by decreasing the threshold stress of MS channels, σ_c (Fig. S4). Finally, in the experiment (11), the actin cortex can be disrupted with blebbistatin to inhibit myosin II contraction and latrunculin A to depolymerize actin filaments. We can model this by lowering the cortical thickness, the elastic modulus of the cortex, and the active stress (see Figs. S5 and S6). In these cases, the volume increases. This change of volume is not the direct result of changing cortical mechanics and tension,

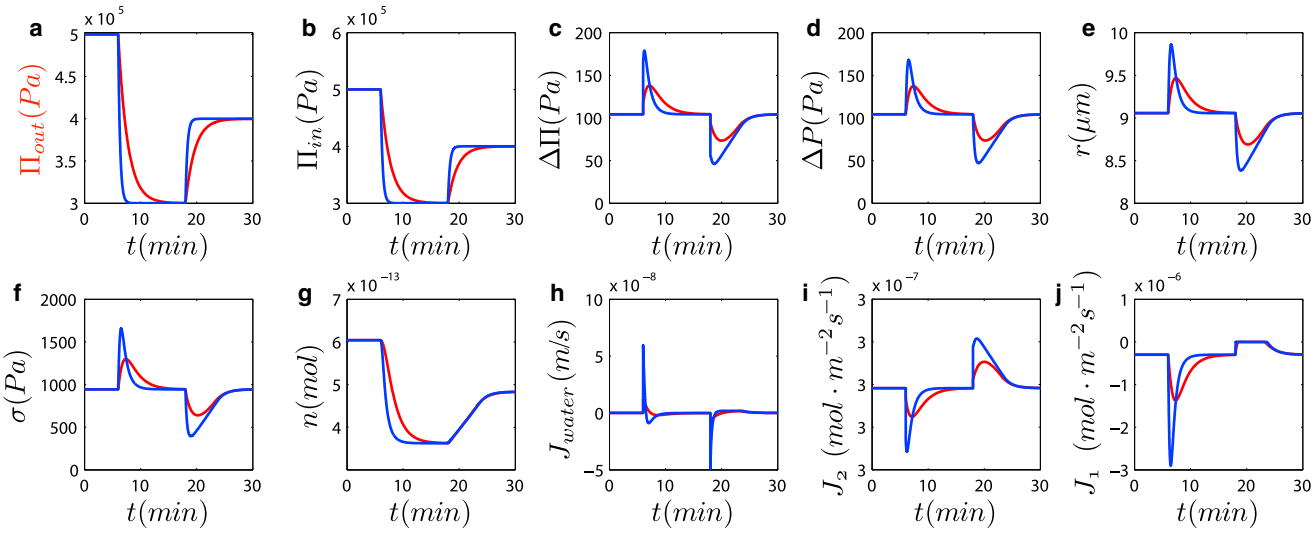

FIGURE 2 Mitotic cells adapt to osmotic shocks. In this figure, we model the experiments of Stewart et al. (11), where metaphase cells are subjected to osmotic shocks. (*a*) A hypotonic shock is introduced at $t = 6$ min followed by a hypertonic shock at $t = 18$ min. The blue and red curves are two wave forms of the osmotic shock. (*b–j*) The response of the cell. Parameters are summarized in Table 1.

but the result of subsequent changes in ion and water permeation. More detailed discussion about how the cell volume is affected by cortex disruption is given in the Supporting Material.

To obtain more insight, we linearize Eq. 5 by assuming that the cortical deformation is small, i.e., $r/r_0 - 1$ is very small. In this case,

$$\frac{K}{2}\left(\frac{r^2}{r_0^2}-1\right) = \frac{K}{2}\left(\frac{r}{r_0}+1\right)\left(\frac{r}{r_0}-1\right) \approx K\left(\frac{r}{r_0}-1\right).$$

Furthermore, we only consider the steady state, so that the viscous term $\eta(2/r)(dr/dt)$ vanishes. The constitutive law for the cortex then becomes $\sigma = K(r/r_0 - 1) - \sigma_a$. In this case, a single static radius,

$$r_s = \left[A_1 + \sqrt{A_1^2 - A_2}\right], \tag{7}$$

exists when $A_1^2 - A_2 \geq 0$, where $A_1 = r_0[\gamma(\Delta\Pi_c r_0 - 2hK) + 2\beta hK(2K + 2\sigma_a + \sigma_c)]/(4\beta hK^2)$ and $A_2 = r_0^2(K + \sigma_a)[-\gamma + \beta(K + \sigma_a + \sigma_c)]/(\beta K^2)$. We see that the steady radius is independent of Π_{out}, so that the cell can adapt to osmotic shocks. The steady radius is regulated by $\Delta\Pi_c$, σ_c, σ_a, r_0, K, and the rate constants. For the

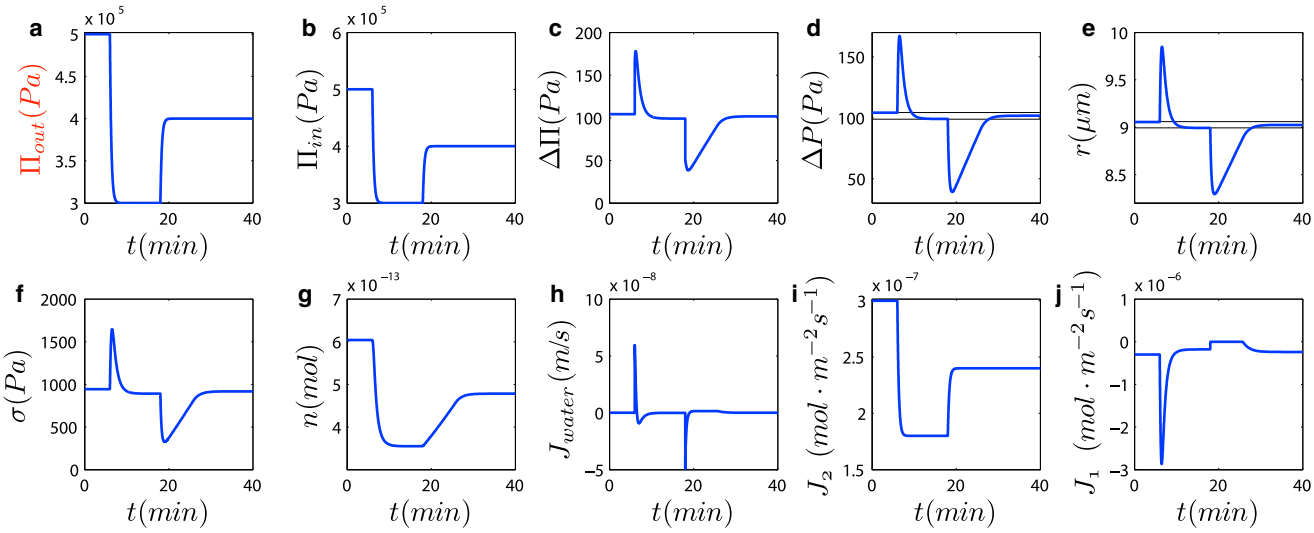

FIGURE 3 Imperfect adaptation to the hypotonic and hypertonic shocks when the critical osmotic pressure difference depends on the osmotic pressure in the growth medium. The steady-state values of r and ΔP become slightly smaller after the hypotonic shock, whereas they become slightly larger after the hypertonic shock. In the simulation, we use $\Delta\Pi_c = 6 \times 10^4 \Pi_{out}$ (see estimation in the main text). Other parameters are summarized in Table 1.

parameter range in living cells (Table 1), $A_1^2 - A_2$ is always positive if $\sigma_a = 0$. However, $A_1^2 - A_2$ could be negative if the absolute value of σ_a is too large compared with K. This regime is unphysical, since in this case the actin filament network is too soft to sustain the contractile force from myosin so that the cell collapses, even when there is significant hydrostatic pressure.

Volume and pressure regulation depend on cortical mechanics, cell types and cell-cycle phase

Indeed, any constitutive law including an elastic part would yield similar adaptation behavior. For example, we can use the neo-Hookean model (30) if we assume the cell cortex is an incompressible hyperelastic material. In this case, $\sigma = \mu(\lambda^2 - 1/\lambda^4) - \sigma_a$, where μ is a material constant and $\lambda = r/r_0$ is the principal stretch along the radial direction. We found that this constitutive law only changes the results quantitatively. However, the cell response changes qualitatively if we assume the cortex is an active viscous fluid. In this case, there is no reference radius, and the passive stress only arises from cortical flow. In the limit where the cortical stress is dominated by σ_a, we can assume that $\sigma_p = 0$, and that σ_a depends only on n. For example, we can use $\sigma = C(n - n_0)$, where C and n_0 are two constants. This relationship models the increase in myosin activity when there is an increase in Ca^{2+} concentration. We find that this constitutive law yields a steady-state radius, but it does not predict adaptation to osmotic shocks (Fig. 4). Therefore, volume and pressure regulation depend on cortex mechanics and an elastic component of the cortex may be required by cells to adapt to osmotic shocks.

The active stress in the cortex, σ_a, is also regulated by signaling networks. For example, the Rho family of GTPases have been implicated in regulating myosin contraction in eukaryotic cells in a calcium-independent manner (31). Therefore, σ_a may be a time-dependent quantity controlled by biochemical signaling networks. It is interesting to consider a more sophisticated theory with an active regulation of σ_a for cells outside of metaphase.

Loading-rate-dependent behavior of living cells under external forces

We have shown that in some parameter range, the cell in our model can adapt to osmotic shocks. For living cells, osmotic shocks are not the only challenge from the environment, they are also under the influence of forces from neighboring cells. Therefore, it is also interesting and important to study how cells regulate their volume and pressure under external forces.

In 1977, Evans and Waugh (32) showed that when a pressure is imposed on the red blood cell by micropipette suction, water molecules are filtered out of the cell so that the osmotic pressure inside the cell increases to oppose the efflux of water. When the net water flux is zero, the cell reaches a steady state. However, the transport of ions controlled by MS channels and ion pumps was not examined. In this article, by considering the transport of both water and ions, we intend to show how the volume and pressure of the cell evolve under external forces. We consider a dynamic indentation experiment where a spherical cell initially in steady state is indented by an AFM cantilever beam at a constant speed with force F (Fig. 5). The indentation depth is d and the radius of the contact area is a. It should be noted that this is different from the experiment setup used by Stewart et al. (11), since the position of the cantilever beam is fixed in the experiment, whereas in this calculation, we consider a dynamic indentation with a constant indentation speed. We assume that there is no friction between the AFM cantilever beam and cell surface and that the cortical stress is uniform in the cortical layer. The cortical stress still obeys the constitutive relation from Eq. 5 after dropping the viscous term.

Similar to Eqs. 1 and 4, the time evolution of the volume and the total number of ions are given by

$$\frac{dV}{dt} = S_{eff} J_{water} \tag{8}$$

and

$$\frac{dn}{dt} = S_{eff}(J_{in} + J_{out}), \tag{9}$$

where S_{eff} is the effective surface area during indentation. Here we assume that there is no ion or water transport across the contact surface. Therefore, $S_{eff} = S - 2\pi a^2$. Replacing S_{eff} by S in Eqs. 8 and 9 only changes the results quantitatively. We also assume that diffusion of ions and mechanical equilibrium are much faster than the transport of water and ions. Therefore, the ion concentration inside the cell is uniform and the cell is always in mechanical equilibrium. The force balance in the cortical layer is given by

$$\Delta P \pi r^2 - F = 2\pi r h \sigma \sin\theta. \tag{10}$$

If the contact angle between cell and beam is zero, the above equation yields $F = \Delta P \pi a^2$. The cell radius, $r(\theta)$, can be solved from Eq. 10 as

$$r(\theta) = a\left[\sqrt{1 + \left(\frac{\sigma h}{\Delta P a}\right)^2 \sin^2\theta} + \frac{\sigma h}{\Delta P a}\sin\theta\right].$$

Since $dz/dr = \tan\theta$, we can obtain $dz/d\theta$. Integrating z over θ, we obtain

$$z = a\left[E_1\left(\theta, -B^2\right) - E_2\left(\theta, -B^2\right)\right] - aB\cos\theta + C, \tag{11}$$

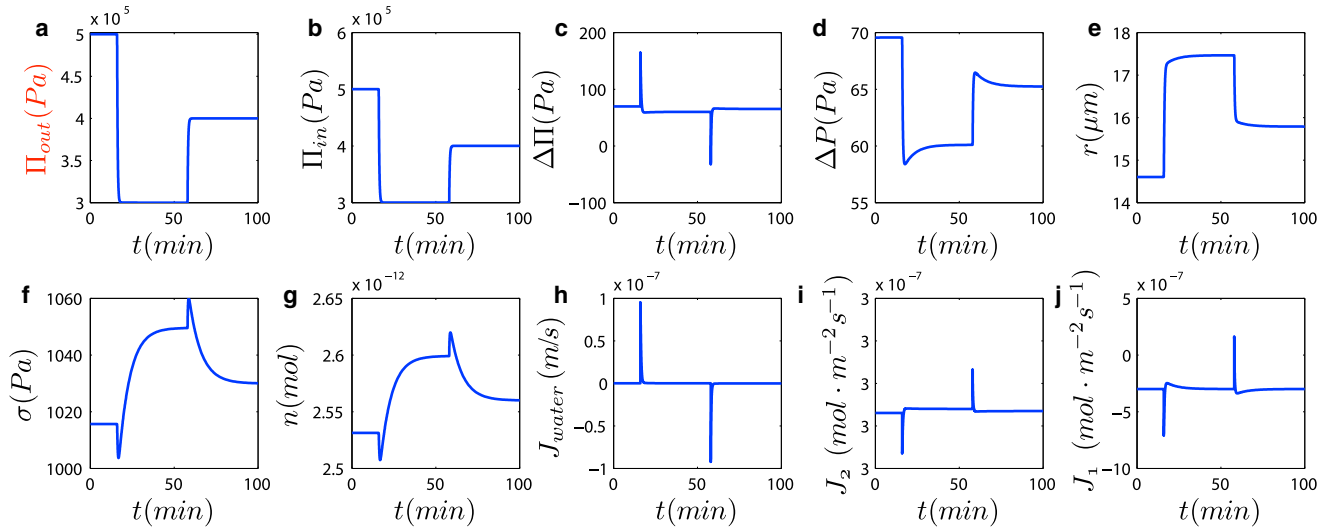

FIGURE 4 The response of the cell to the hypotonic and hypertonic shocks when the constitutive law of the cortex, $\sigma = C(n - n_0)$, is used. In the calculation, $C = 5 \times 10^{14}$ Pa/mol and $n_0 = 5 \times 10^{-13}$ mol are used. Other parameters are summarized in Table 1.

where $B = \sigma h/\Delta Pa$ is an unknown dimensionless variable, which must be solved from another condition. $E_1(\theta, m) = \int_0^\theta \sqrt{1 - m\sin^2\phi}\, d\phi$ and $E_2(\theta, m) = \int_0^\theta (1/\sqrt{1 - m\sin^2\phi})\ d\phi$ are the incomplete elliptic integrals of the first and second kind, respectively. The boundary conditions are given by

$$\begin{aligned} z &= 0 \qquad (\text{at } \theta = 0) \\ z &= \frac{(2r_0 - d)}{2} \quad \left(\text{at } \theta = \frac{\pi}{2}\right) \end{aligned}. \tag{12}$$

From the boundary conditions, we have

$$\frac{(2r_0 - d)}{2} = a\left[E_1\left(\frac{\pi}{2}, -B^2\right) - E_2\left(\frac{\pi}{2}, -B^2\right)\right] + aB. \tag{13}$$

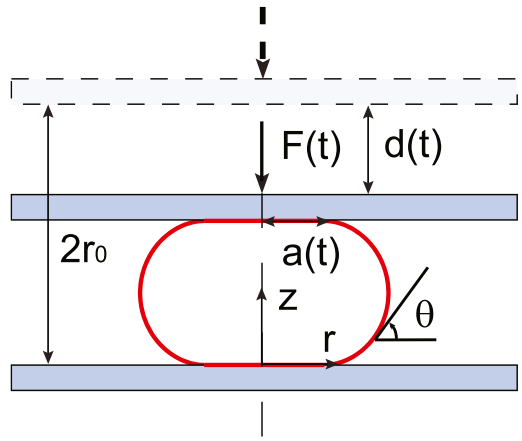

FIGURE 5 Dynamic indentation of a, symmetric cell using an AFM cantilever beam at a constant indentation speed. $F(t)$ is the indentation force, $d(t)$ is the indentation depth, and $a(t)$ is the contact area. The cell shape is cylindrically symmetric and is described by functions $(r(\theta, t), z(\theta, t))$.

In terms of B and a, the surface area and volume of the cell are

$$S_{eff} = 4\pi(aB)^2\left[\frac{2}{B}E_1\left(\frac{\pi}{2}, -B^2\right) - \frac{1}{B}E_2\left(\frac{\pi}{2}, -B^2\right) + 2\right]. \tag{14}$$

and

$$\begin{aligned} V = \frac{2\pi}{3}(aB)^3\Bigg[&\frac{1}{B}\left(\frac{1}{B^2} + 8\right)E_1\left(\frac{\pi}{2}, -B^2\right) \\ &-\frac{1}{B}\left(\frac{1}{B^2} + 4\right)E_2\left(\frac{\pi}{2}, -B^2\right) + \left(\frac{3}{B^2} + 8\right)\Bigg]. \end{aligned} \tag{15}$$

By solving the coupled equations above (Eqs. 8, 9, and 13–15), we can obtain the contact area, volume, indentation force, and other variables. In the simulation, we assume the indentation depth is $d = kt$, where k is the indentation speed. We find that the indentation force, F, depends strongly on the indentation speed, k, especially when the deformation is large (Fig. 6 *c*). The dependence comes from the flow of water and ions (Fig. 6, *j–l*), which leads to shrinkage of the cell (Fig. 6 *d*). If the indentation speed is comparable to or smaller than the speed of water transport, more MS channels are open as the cortical stress increases with indentation. Both water and ions flow out of the cell, so that the cell shrinks. In contrast, if the indentation is much faster than the flow of water and ions, water and ion flows are negligible and the cell volume is nearly conserved. Therefore, the indentation force becomes much larger. We found that for small indentation speed ($k = 0.01\ \mu$m/s and $k = 0.1\ \mu$m/s), the cell volume can decrease significantly when the indentation depth, d, is large (Fig. 6 *d*, *red* and *green curves*), whereas for the large

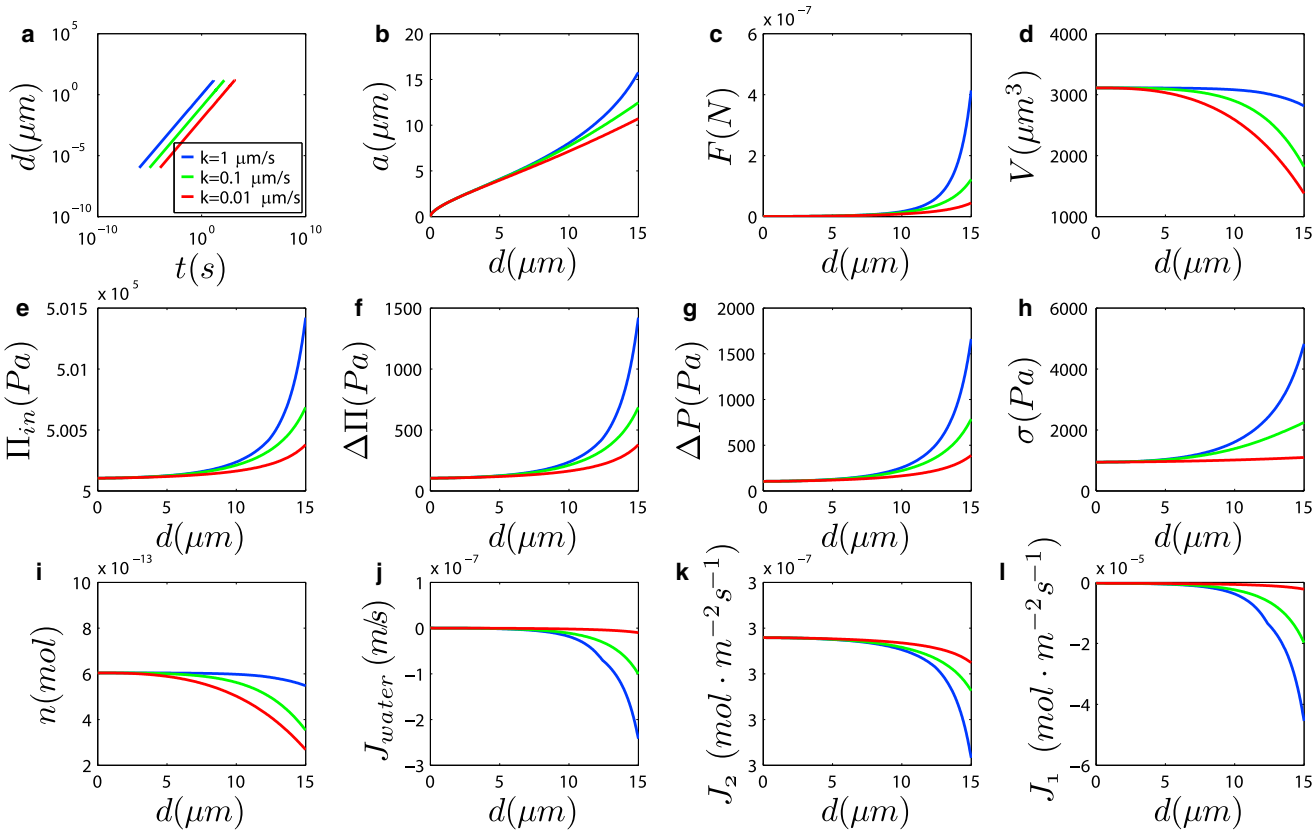

FIGURE 6 Simulation results for the dynamic indentation of a cell using an AFM cantilever beam at a constant indentation speed. The cell is indented at three speeds: $k = 1\ \mu$m/s, $k = 0.1\ \mu$m/s, and $k = 0.01\ \mu$m/s. Other parameters used are summarized in Table 1. Note that at fast indentation speeds, 1 μm/s, the cell essentially maintains a constant volume. However, when the deformation speed is slower, the volume change is significant.

indentation speed $k = 1\ \mu$m/s, the cell volume is almost conserved in our calculation (Fig. 6 *d*, *blue curve*). This is consistent with the experimental observation that the cell volume is nearly conserved for the indentation speed $k = 3\ \mu$m/s used in the experiments (33). Our predictions might also be useful to understand the cell monolayer stretching experiment (34), where the cell monolayer (~1 mm long) is stretched at strain rates between 0.5%/s and 5%/s. In a study by Harris et al. (34), the loading rate was between 5 and 50 μm/s, which is much higher than the loading rate used in our calculation. For such high loading rates, the cell volume should be nearly conserved, as we predict in this model; cells should appear to be incompressible (33,34). In contrast, the flow of water and the corresponding cell volume decrease have been observed when a red blood cell is suctioned by a micropipette and suctioning is maintained for a long period (32). Unfortunately, the pressure used in experiments was quite small (roughly several kPa) so that the volume change is small. Therefore, more experimental measurements of the cell-volume change under large forces and low indentation speeds are required to further verify our predictions. We note, however, that in most physiologically important settings, such as during embryonic development, the strain rate is likely to be quite small (35), since most tissues change size over many hours. Therefore, the timescale of deformation is an important variable. Also, it should be noted that the cell membrane tension can decrease not only through the openings of more MS channels and the efflux of water and ions, but also by formation of blebs. The coupling between the blebbing dynamics and cell-volume regulation would be another interesting topic for further exploration.

We see that during external application of forces, living cells can actively regulate their volume and pressure in reaction to the external loading, and therefore cannot be treated as a static balloonlike object. The measured cell stiffness must be carefully interpreted, since it strongly depends on the loading rate and experimental environment. A characteristic of viscoelasticity is that the stress depends on the strain rate. Therefore, this rate-dependent behavior due to volume and pressure regulation can contribute to the observed viscoelastic response of living cells (6,9). This rate-dependent behavior due to the transport of water may be also important for other situations where cells undergo large deformation, e.g., cell division. Experiments have shown that the efflux of water and ions leads to a dramatic volume decrease as glioma cells progress through mitosis, so that at division, all cells have a common volume (36). However,

when the constriction speed of the contractile ring is fast compared to water and ion transport, cells might not show a detectable volume change (37). Also, measurements of cell volume in these experiments (11,36,37) were not very accurate, especially when cells were adhered to substrate. Therefore, additional careful measurements should be performed on spherical cells in suspension to monitor cell-volume changes when the constriction speed of the contractile ring is slow.

CONCLUSION AND DISCUSSION

For eukaryotic animal cells, cell volume and cell shape are variables that are controlled by a combination of the actomyosin cytoskeleton, MS channels, and ion pumps. The action of these machines are coupled together to achieve cell-volume control. In this article, we have developed the basic framework for volume and pressure regulation in mitotic cells or cells in suspension. Our results can explain the experiment by Stewart et al (11) qualitatively. We showed that active stress from cytoskeletal motors is not sufficient to control cell volume. MS channels and active ion and small-molecule pumps are also important. The adaptation dynamics also depends strongly on cortical mechanics, which cells can actively regulate. Our model currently describes the single-species case. For a real cell, multiple solutes and multiple channels and pumps must be considered. The overall dynamics is likely to be quite rich.

We also examined a model of dynamic cell indentation to show that the indentation force depends strongly on the indentation speed, especially when the deformation is large. We showed that not only osmotic shocks but also mechanical stress can influence water and ion transport. In addition, adhesions to 2D substrates can be regarded as another kind of force on cells. Therefore, our model also has consequences for cell shape and volume change during cell adhesion and spreading on 2D substrates of varying stiffness and adhesion energy. However, the relevant data are still lacking, and new experiments are therefore required to fully explore this regime. Experiments also showed that osmotic shocks can drive a pearling instability in axons (38), which suggest additional shape instabilities connected to water and ion permeation.

Finally, our model also has important implications for cell motility, where cells actively change their shape by extending protrusions at the front and retracting at the rear. On 2D substrates, these shape changes have been mainly attributed to actin cytoskeletal dynamics. However, osmotic stress can also greatly influence cell migration for many cell types (1). It has also been demonstrated that a fluid flow in a tube can be driven by an osmotic pressure difference generated by a reaction diffusion system (39). Based on our simple model of volume and pressure regulation developed in this article, we propose that by controlling the influx and efflux of water and ions, cells can achieve migration in confined spaces. This migration mechanism might explain why metastatic breast cancer cells migrate through narrow channels even when actin polymerization, Rho/ROCK- or myosin-II-dependent contractility, or integrin function are inhibited (40). However, this proposed mechanism and the precise roles of water, cytoskeleton, membrane proteins, and membrane tension during motility in different kinds of cells still require further elucidation.

A fundamental question raised by our model is, what is the appropriate constitutive relation for the cell cortex? The answer probably varies from cell to cell, and it also may depend strongly on the phase of the cell cycle. Indeed during typical osmotic-shock experiments, the cell can lyse, suggesting that a soft and liquidlike cortex will balloon. In addition, signaling networks with unexplored control algorithms can regulate the active stress in the cell cortex. Therefore, further explorations of this model in these contexts are needed.

SUPPORTING MATERIAL

Six figures and additional explanation of the model, are available at http://www.biophysj.org/biophysj/supplemental/S0006-3495(13)00700-5.

The authors acknowledge helpful discussions with Frank Jülicher and Elisabeth Fischer- Friedrich. S.X.S also gratefully acknowledges support from the Max Planck Institute for Physics of Complex Systems and the Alexander von Humboldt foundation.

This work has been supported by National Institutes of Health grants 1U54CA143868-01, 1R01GM075305, and NSF PHY-1205795.

REFERENCES

1. Hoffmann, E. K., I. H. Lambert, and S. F. Pedersen. 2009. Physiology of cell volume regulation in vertebrates. *Physiol. Rev.* 89:193–277.
2. Clark, A. G., and E. Paluch. 2011. Mechanics and regulation of cell shape during the cell cycle. *Cell Cycle Dev.* 53:31–73.
3. Salbreux, G., G. Charras, and E. Paluch. 2012. Actin cortex mechanics and cellular morphogenesis. *Trends Cell Biol.* 22:536–545.
4. Evans, E., and A. Yeung. 1989. Apparent viscosity and cortical tension of blood granulocytes determined by micropipet aspiration. *Biophys. J.* 56:151–160.
5. Sedzinski, J., M. Biro, …, E. Paluch. 2011. Polar actomyosin contractility destabilizes the position of the cytokinetic furrow. *Nature.* 476:462–466.
6. Li, Q. S., G. Y. Lee, …, C. T. Lim. 2008. AFM indentation study of breast cancer cells. *Biochem. Biophys. Res. Commun.* 374:609–613.
7. Sun, Y., K. T. Wan, …, B. J. Nelson. 2003. Mechanical property characterization of mouse zona pellucida. *IEEE Trans. Nanobioscience.* 2:279–286.
8. Fabry, B., G. N. Maksym, …, J. J. Fredberg. 2001. Scaling the microrheology of living cells. *Phys. Rev. Lett.* 87:148102.
9. Wottawah, F., S. Schinkinger, …, J. Käs. 2005. Optical rheology of biological cells. *Phys. Rev. Lett.* 94:098103.
10. Moeendarbary, E., L. Valon, …, G. T. Charras. 2013. The cytoplasm of living cells behaves as a poroelastic material. *Nat. Mater.* 12:253–261.
11. Stewart, M. P., J. Helenius, …, A. A. Hyman. 2011. Hydrostatic pressure and the actomyosin cortex drive mitotic cell rounding. *Nature.* 469:226–230.

12. Keren, K., P. T. Yam, …, J. A. Theriot. 2009. Intracellular fluid flow in rapidly moving cells. *Nat. Cell Biol.* 11:1219–1224.

13. Charras, G., and E. Paluch. 2008. Blebs lead the way: how to migrate without lamellipodia. *Nat. Rev. Mol. Cell Biol.* 9:730–736.

14. Loitto, V. M., T. Forslund, …, M. Gustafsson. 2002. Neutrophil leukocyte motility requires directed water influx. *J. Leukoc. Biol.* 71:212–222.

15. Oster, G., and A. Perelson. 1987. The physics of cell motility. *In* Cell Behavior: Shape, Adhesion, and Motility. J. Heaysman, C. Middleton, and F. Watt, editors. Company of Biologists, Cambridge, United Kingdom. pp 35–54.

16. Gauthier, N. C., T. A. Masters, and M. P. Sheetz. 2012. Mechanical feedback between membrane tension and dynamics. *Trends Cell Biol.* 22:527–535.

17. Tinevez, J. Y., U. Schulze, …, E. Paluch. 2009. Role of cortical tension in bleb growth. *Proc. Natl. Acad. Sci. USA.* 106:18581–18586.

18. Finkelstein, A. 1987. Water Movement through Lipid Bilayers, Pores and Plasma Membranes. Wiley lnterscience, New York.

19. Agre, P. 2006. The aquaporin water channels. *Proc. Am. Thorac. Soc.* 3:5–13.

20. Kung, C. 2005. A possible unifying principle for mechanosensation. *Nature*. 436:647–654.

21. Marshall, W. S., and M. Grosell. 2006. Ion transport, osmoregulation, and acid-base balance. *In* The physiology of fishes. D. H. Evans and J. B. Claiborne, editors. Taylor and Francis, Boca Raton, FL. pp 177–230.

22. Dubyak, G. R. 2004. Ion homeostasis, channels, and transporters: an update on cellular mechanisms. *Adv. Physiol. Educ.* 28:143–154.

23. Sukharev, S. I., W. J. Sigurdson, …, F. Sachs. 1999. Energetic and spatial parameters for gating of the bacterial large conductance mechano-sensitive channel, MscL. *J. Gen. Physiol.* 113:525–540.

24. Glitsch, H. G., and A. Tappe. 1995. Change of Na^+ pump current reversal potential in sheep cardiac Purkinje cells with varying free energy of ATP hydrolysis. *J. Physiol.* 484:605–616.

25. Bonting, S. L., and J. J. H. H. M. de Pont, editors. 1981. New Comprehensive Biochemistry. Volume 2: Membrane Transport. Elsevier, Philadelphia.

26. Jülicher, F., K. Kruse, …, J. F. Joanny. 2007. Active behavior of the cytoskeleton. *Phys. Rep.* 449:3–28.

27. Kruse, K., J. F. Joanny, …, K. Sekimoto. 2005. Generic theory of active polar gels: a paradigm for cytoskeletal dynamics. *Eur. Phys. J. E Soft Matter.* 16:5–16.

28. Wan, K. T., and K. K. Liu. 2001. Contact mechanics of a thin-walled capsule adhered onto a rigid planar substrate. *Med. Biol. Eng. Comput.* 39:605–608.

29. Koay, E. J., A. C. Shieh, and K. A. Athanasiou. 2003. Creep indentation of single cells. *J. Biomech. Eng.* 125:334–341.

30. Ogden, R. W. 1997. Non-Linear Elastic Deformations. Dover, Mineola, NY.

31. Katoh, K., Y. Kano, and Y. Noda. 2011. Rho-associated kinase-dependent contraction of stress fibres and the organization of focal adhesions. *J. R. Soc. Interface.* 8:305–311.

32. Evans, E. A., and R. Waugh. 1977. Osmotic correction to elastic area compressibility measurements on red cell membrane. *Biophys. J.* 20:307–313.

33. Harris, A. R., and G. T. Charras. 2011. Experimental validation of atomic force microscopy-based cell elasticity measurements. *Nanotechnology.* 22:345102.

34. Harris, A. R., L. Peter, …, G. T. Charras. 2012. Characterizing the mechanics of cultured cell monolayers. *Proc. Natl. Acad. Sci. USA.* 109:16449–16454.

35. Blanchard, G. B., A. J. Kabla, …, R. J. Adams. 2009. Tissue tectonics: morphogenetic strain rates, cell shape change and intercalation. *Nat. Methods.* 6:458–464.

36. Habela, C. W., and H. Sontheimer. 2007. Cytoplasmic volume condensation is an integral part of mitosis. *Cell Cycle.* 6:1613–1620.

37. Robinson, D. N., G. Cavet, …, J. A. Spudich. 2002. Quantitation of the distribution and flux of myosin-II during cytokinesis. *BMC Cell Biol.* 3:4.

38. Pullarkat, P. A., P. Dommersnes, …, A. Ott. 2006. Osmotically driven shape transformations in axons. *Phys. Rev. Lett.* 96:048104.

39. Atzberger, P. J., S. Isaacson, and C. S. Peskin. 2009. A microfluidic pumping mechanism driven by non-equilibrium osmotic effects. *Physica D.* 238:1168–1179.

40. Balzer, E. M., Z. Tong, …, K. Konstantopoulos. 2012. Physical confinement alters tumor cell adhesion and migration phenotypes. *FASEB J.* 26:4045–4056.

41. Pesen, D., and J. H. Hoh. 2005. Micromechanical architecture of the endothelial cell cortex. *Biophys. J.* 88:670–679.

42. Kuznetsova, T. G., M. N. Starodubtseva, …, R. I. Zhdanov. 2007. Atomic force microscopy probing of cell elasticity. *Micron.* 38:824–833.

43. Grosell, M. 2006. Intestinal anion exchange in marine fish osmoregulation. *J. Exp. Biol.* 209:2813–2827.

44. Larsen, E. H., N. Møbjerg, and R. Nielsen. 2007. Application of the Na^+ recirculation theory to ion coupled water transport in low- and high-resistance osmoregulatory epithelia. *Comp. Biochem. Physiol. A Mol. Integr. Physiol.* 148:101–116.

45. Marrink, S. J., and H. J. C. Berendsen. 1994. Simulation of water transport through a lipid membrane. *J. Phys. Chem.* 98:4155–4168.

46. Benga, G., V. I. Pop, …, V. Borza. 1990. On measuring the diffusional water permeability of human red blood cells and ghosts by nuclear magnetic resonance. *J. Biochem. Biophys. Methods.* 21:87–102.

Cellular pressure and volume regulation and implications for cell mechanics: supplemental information

Hongyuan Jiang[1] and Sean X. Sun[1]

[1] *Department of Mechanical Engineering and Johns Hopkins Physical Sciences-Oncology Center, Johns Hopkins University, Baltimore MD 21218, USA*

(Dated: June 4, 2013)

Fig. S1 and S2 show the relevant quantities in the model during relaxation to steady state cell radius. Fig. S1 shows the relaxation to the pump and leak steady state, Fig. S2 shows the relaxation to the static steady state.

Fig. S3 models the experiments from Stewart et al, where drugs were used to disrupt ion pumps. We model this change by decreasing the critical osmotic pressure for the ion pumps $\Delta\Pi_c$, and decreasing the threshold stress, σ_c, of mechanosensitive channels. Results show that the cell radius decreases.

Fig. S4 also models the experiments from Stewart et al, where drugs were used to increase the permeability of the cell membrane to ions. In our model, this can be described by either decreasing the threshold stress, σ_c, of mechanosensitive channels, or increasing the ion permeation constant β. Both changes give similar results as shown in Fig. S4, and the cell radius decreases.

Fig. S5 and S6 shows the effects of myosin contractility and the actin cortex. In the experiment of Ref. 11, the cortex can be disrupted with blebbistatin to inhibit myosin II contraction, and latrunculin A to depolymerize actin filaments (the case of Fig. 3f in Ref. 11). The volume is increased by about 7∼8%, which is equivalent to 2∼3% increase of cell radius. The effect of blebbistatin is to decrease the amplitude of active stress σ_a. Latrunculin A can affect cortex in two aspects: decrease the elastic modulus K and decrease the thickness of the cortex h. Our simulation (Fig. S5) shows that if we decrease the elastic modulus K by 50% (from 6 KPa to 3 KPa) and keep h as a constant (0.5 μm), the static cell radius increases 13% (from 9.06 μm to 10.24 μm). Our simulation (Fig. S6) also shows that if we decrease the cortical thickness h by 50% (from 0.5 μm to 0.25 μm) and keep K as a constant (6 KPa), the static cell radius only increases 2.8% (from 9.06 μm to 9.31 μm). This indicates that the static radius is insensitive to h and our simulation can fit the experimental results. Thus we see that the sensitivities of the static cell radius with respect to h and K are different. How latrunculin A affects the cortical thickness h and the elastic modulus K is still unclear. Furthermore, h and K also depend on the dose of latrunculin A and the cortex may not be depolymerized completely for low concentration of latrunculin A.

In our model, the static cell radius goes to infinity as K approaches zero since no structure can resist the hydrostatic pressure difference in this case. In reality, however, the elastic modulus is unlikely to decrease too much since the elastic component in our model may also come from other sources besides the cortex, such as the mitotic spindle, intermediate filaments and the cell membrane. How much each of them contributes to the observed cell elasticity is still unclear. If we only depolymerize one of them, K should not decrease very much. Even if the cortex, mitotic spindle, intermediate filaments are all depolymerized simultaneously, the cell membrane can still contribute to K. From experimental studies of osmotic swelling and lysis of lipid vesicles, the Young's modulus of tout lipid membrane is in the range of 10^7Pa, which is larger than the elastic modulus of the cortex [1, 2]. Even for these artificial lipid membranes, the volume change after osmotic shocks is not very large (¡ 10%) [2]. However, it should also be noted that the contribution of the cell membrane to K should not be very large due to the existence of excess membrane.

Finally, although we argued that any elastic constitutive law with a reference radius would yield similar adaptation behavior, different elastic constitutive laws will yield different sensitivity of the cell radius with respect to K. For example, in our simulation we use the constitutive law $\sigma = \frac{K}{2}\left(\frac{S}{S_0} - 1\right) - \sigma_a$ (Eq. 5 in our main text). While in order to obtain more insights, we linearized this equation by assuming the cortical deformation is small. So the constitutive law for the cortex becomes $\sigma = K(r/r_0 - 1) - \sigma_a$. We found this linear constitutive law is more sensitive than the constitutive law $\sigma = \frac{K}{2}\left(\frac{S}{S_0} - 1\right) - \sigma_a$ with respect to K. In our paper, we explored several constitutive laws. However, as we have discussed in the main text, the constitutive law of the cortex still requires more experimental and theoretical investigation.

[1] F. R. Hallett, J. Marsh, B. G. Nickel, J. M. Wood, Biophys. J. **64**:435-42(1993).

[2] W. Li, T. S. Aurora, T. H. Haines, H. Z. Cummins. Biochemistry. **25**:8220-9 (1986).

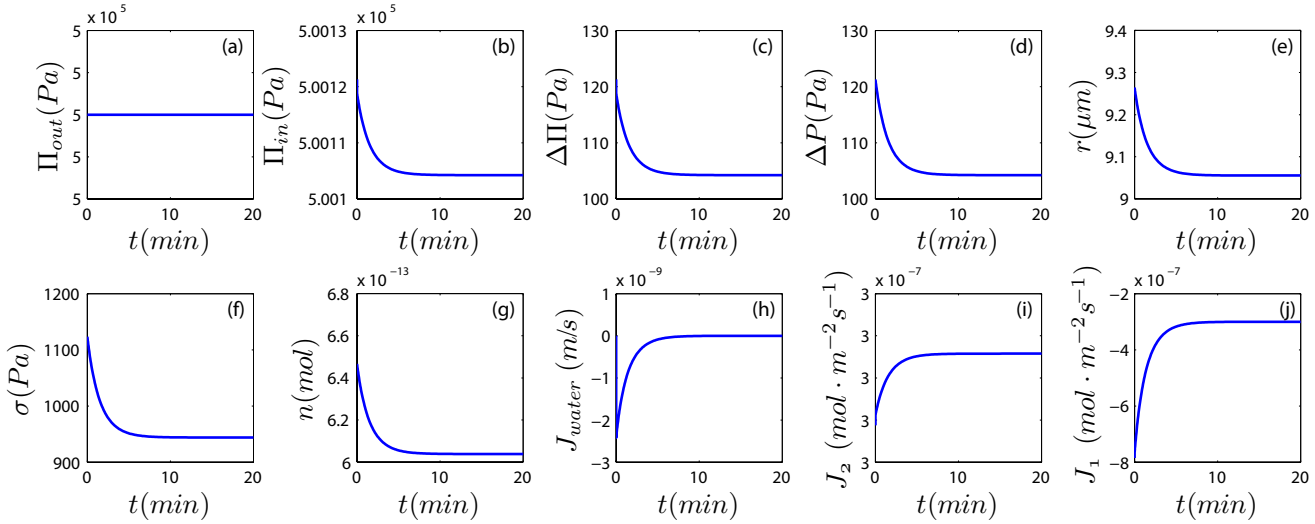

FIG. S1: *For parameters that satisfy Eq. 10, cells pump and leak (Fig. 1(d)). At the steady state, the influx and efflux of ions are equal and opposite, but not vanishing. Parameters used are summarized in the Table 1.*

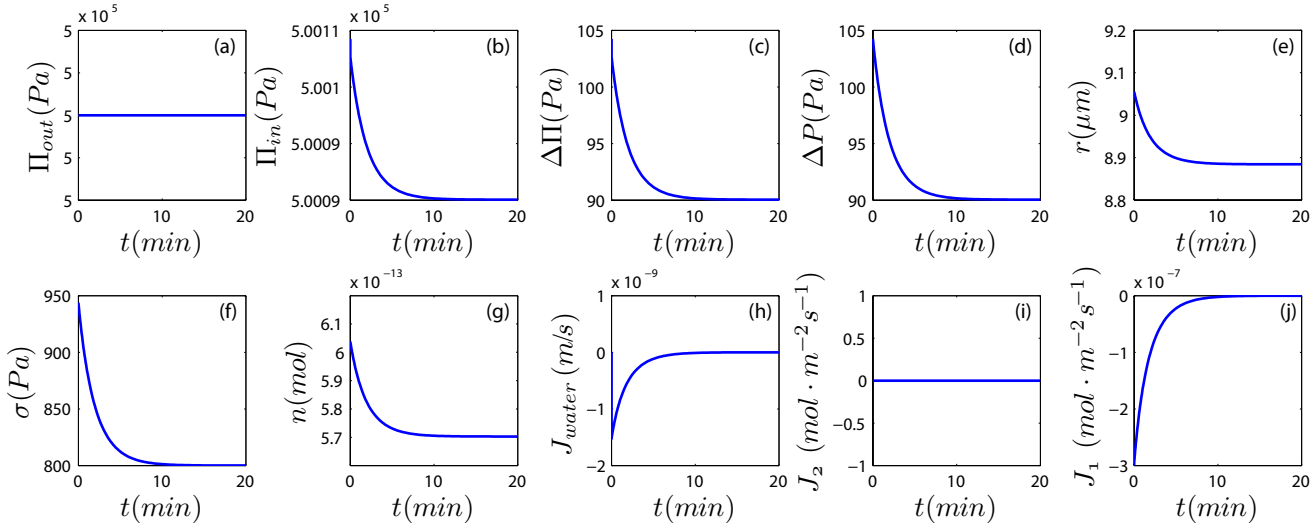

FIG. S2: *For parameters that do not satisfy Eq. 10, cells can reach a static equilibrium (Fig. 1(d)). At the steady state, the influx and efflux of ions are always zero. In the calculation,* $\Delta\Pi_c = 50Pa$ *and other parameters used are summarized in the Table 1.*

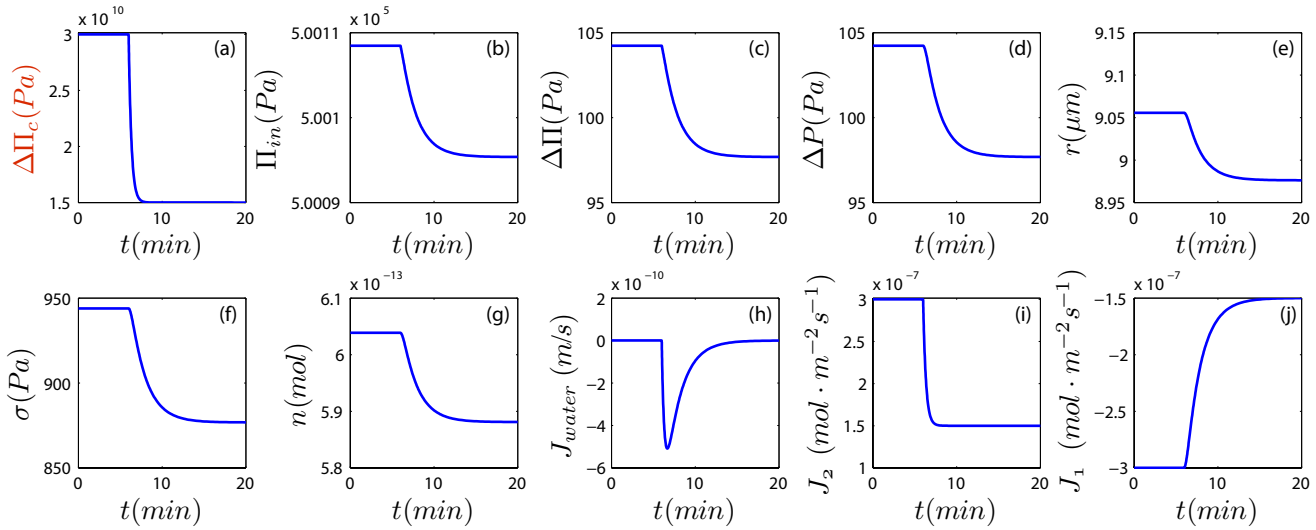

FIG. S3: *Modeling the experiment of Stewart et al., where Na^+/H^+ ion pumps were blocked using a drug. (a) We model this by decreasing the value of $\Delta\Pi_c$ at $t = 6$ min. (b)-(j) The response of the cell.*

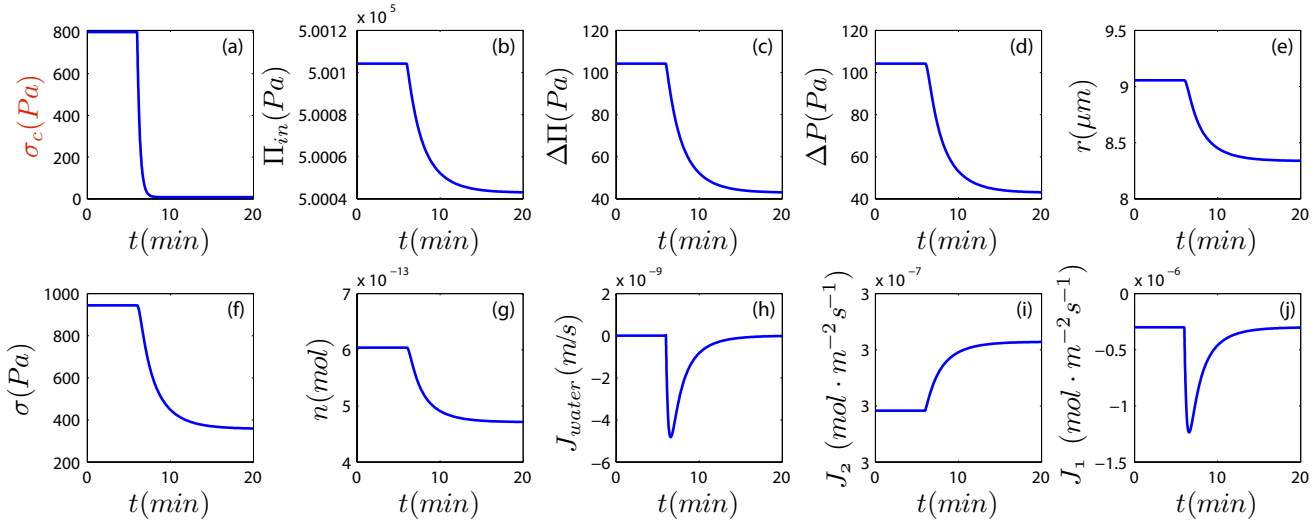

FIG. S4: *Modeling the experiment of Stewart et al., where they used a drug to render the cell membrane permeable to ions. (a) We model this by decreasing the threshold stress of MS channels, σ_c, at t=6 min. (b)-(j) The response of the cell.*

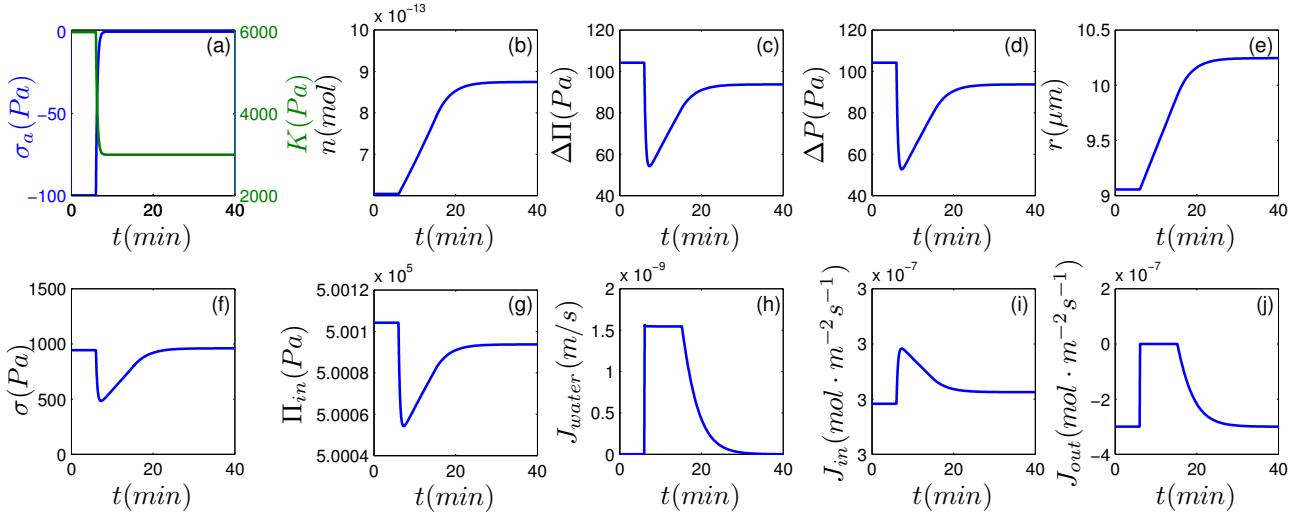

FIG. S5: *(a) At t=6 min, lowering the amplitude of σ_a to simulate the inhibition of myosin II contraction, and decreasing the elastic modulus of the cortex K by 50% to simulate the depolymerizing actin filament. (b)-(j) The response of the cell. The static cell radius increases 13%.*

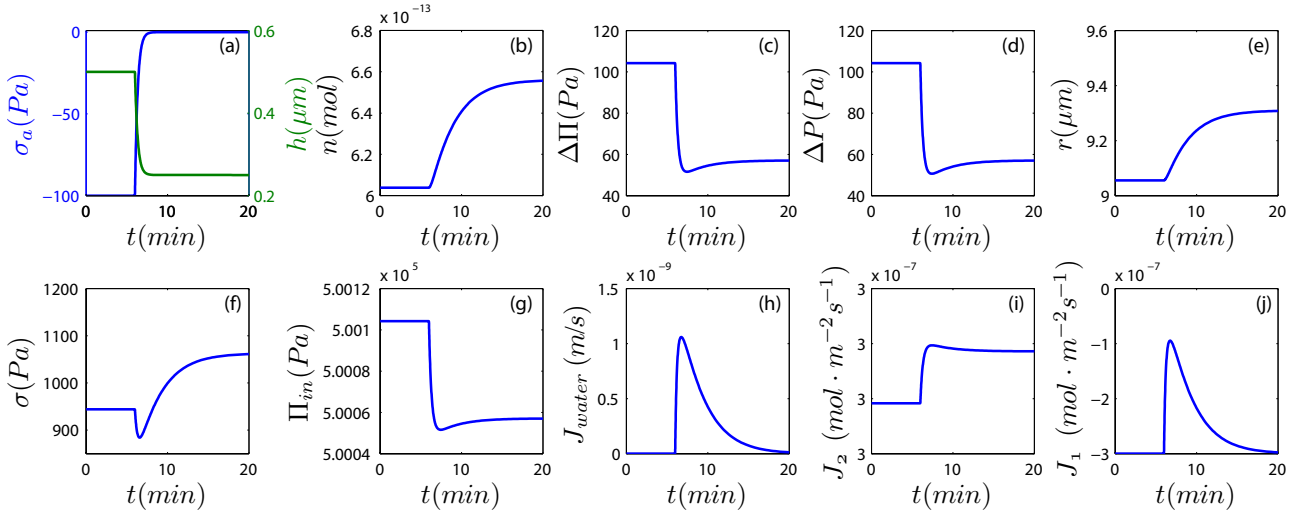

FIG. S6: *(a) At t=6 min, lowering the amplitude of σ_a to simulate the inhibition of myosin II contraction, and decreasing the cortex thickness h by 50% to simulate the depolymerizing actin filament. (b)-(j) The response of the cell. The static cell radius only increases 2.8%.*